Thin Solid Films 558 (2014) 67–74

Contents lists available at ScienceDirect

Thin Solid Films

journal homepage: www.elsevier.com/locate/tsf

Formation of Ti(III) and Ti(IV) states in Ti_3O_5 nano- and microfibers obtained from hydrothermal annealing of C-doped TiO_2 on Si

Nair Stem [a,*], Michele L. de Souza [b], Dalva Lúcia Araújo de Faria [b], Sebastião G. dos Santos Filho [a]

[a] Laboratório de Sistemas Integráveis (LSI), Escola Politécnica, Universidade de São Paulo, Av. Prof. Luciano Gualberto 158, 05508900 São Paulo, SP, Brazil
[b] Laboratório de Espectroscopia Molecular (LEM), Instituto de Química, Universidade de São Paulo, Av. Prof. Lineu Prestes 748, 05508900 São Paulo, SP, Brazil

ARTICLE INFO

Article history:
Received 12 December 2012
Received in revised form 28 January 2014
Accepted 21 February 2014
Available online 28 February 2014

Keywords:
Chemical bonds
Nanofibers
Ti_3O_5
TiO_2
Hydrothermal annealing

ABSTRACT

In this work, it is investigated the formation of Ti(III) and Ti(IV) states at the surface and in the bulk of the Ti_3O_5 material grown as meshes of nano- and micro-fibers obtained from hydrothermal annealing of C-doped TiO_2 on Si. The topography and distribution of the fibers in the meshes were characterized by atomic force microscopy. When the fiber distribution was more compact, a higher photoluminescence signal at 850 nm (1.46 eV) was obtained, indicating the presence of a higher number of defects corresponding to the Ti(III) sites. From X-ray photoelectron spectroscopy, it was obtained a Ti(III)/Ti(IV) ratio much lower than the expected value for the Ti_3O_5 phase (2 Ti(III): 1 Ti(IV)). The discrepancy was mainly attributed to the reaction of surface Ti(III) states of the Ti_3O_5 fibers with water during the hydrothermal annealing, resulting in surface Ti(IV) with −OH radicals. On the other hand, X-ray photoelectron spectroscopy also indicated that substitutional and interstitial carbon atoms coexist, elemental carbon exists in the samples due to the co-deposition process and, as a result, the carbon inside of the TiO_2 rutile lattice is acting as one of the precursors for the formation of Ti_3O_5.

1. Introduction

The chemical reduction of TiO_2 has been of great interest for several different uses, including photocatalysis, solar cells and biomedical applications [1–4]. For biomedical applications, the Ti(III) states from reduced TiO_2 have been shown to be electronically modified and to have enhanced hydrophilicity; good adsorption properties for enzyme proteins and other adsorbates; and high biocompatibility [5–8]. The chemical reduction of TiO_2 have been obtained by different methods such as argon bombardment, electron beam exposure, and thermal annealing in different environments, as well as chemically via catalytic reactions on metal surfaces, among others [5,6].

According to Ladaini et al. [9], rutile titanium dioxide and nearly stoichiometric TiO_{2-x} are stable forms of TiO_2 with a small number of point defects. However, as the number of point defects increases, rearrangements in the crystalline structure (crystallographic shear planes, CSP) are observed to accommodate them. The point defects are often correlated to oxygen deficiencies, such as Ti interstitials and oxygen vacancies or a combination of both, and they are also associated with oxygen diffusion or doping [10–16]. Oxygen vacancies can be either doubly or singly ionized, resulting in titanium interstitials in either the Ti(III) or Ti(IV) states, depending on the reaction [17]. However, when the concentrations of these vacancies in the CSP increase enough, the formation of Ti_nO_{2n-1} (Ti_3O_5, Ti_4O_7, Ti_5O_9, Ti_6O_{11}, etc.) compounds is possible [12]. The distance between oxygen–oxygen planes in the CSP of Ti_nO_{2n-1} phases is smaller, comprises TiO_6 octahedra that are joined by sharing edges and corners to form slabs of a rutile type structure [17–19], and sometimes forms different crystalline structures with distinct space groups and specific cell volumes [20]. In the case of Ti_3O_5 phase, the proportion of Ti(III) and Ti(IV) states is approximately 2 to1 [18].

Ti_nO_{2n-1} phases have been synthesized from titania activated with additives (C, Nb, V, Fe. etc.) and thermally treated in inert or reducing atmospheres over a wide range of temperatures (1000 °C–1500 °C) [19–22]. All Ti_nO_{2n-1} phases present a triclinic system with very similar lattice parameters (α, β, γ, δ, and more recently, λ phases); however, it is difficult to obtain a pure monophase product and identify the obtained compounds [13,14,23–29].

The α-phase is generally obtained at very high temperatures (1473 °C), has a CmCm space group and it is metastable until approximately 698 °C, where the β-phase is formed (C2/m space group) [29]. If the β-phase is heated up to 773 °C, it can be transformed into the α-phase (the so-called Anosovite structure). In contrast, slow cooling of the α-phase can result in the formation of the γ-phase (having an isomorphous structure that belongs to the I2/c space group), and at approximately 506 °C, the γ-phase can also be transformed into the δ-phase (P2/c space group) [25]. An important consideration is that

* Corresponding author.
E-mail address: nairstem@hotmail.com (N. Stem).

http://dx.doi.org/10.1016/j.tsf.2014.02.077
0040-6090/

the β-phase [27] and λ-phase [28] belong to the same space group, C2/m, but present different unit cell volumes of 0.3546 nm^3 and 0.3758 nm^3, respectively. In particular, the λ-phase of Ti_3O_5 has recently been shown to have a photoreversible phase transition at room temperature, and it can absorb light over a wide range of wavelengths (from the UV to the near infra-red) [28].

In a previous work [30], Ti_3O_5 was produced from C-doped TiO_2 on Si via hydrothermal annealing by using wet nitrogen (0.8% wt H_2O) under 1000 °C temperature. In this case, the TiO_2 rutile phase is initially formed from amorphous TiO_2 on Si and, in following, the Ti_3O_5 meshes of nano- and microfibers are grown for at least 3 wt.% of carbon doping. This route was chosen because carbon and water vapor play crucial roles in the achievement of Ti_3O_5 by forming defects and oxygen vacancies in the rutile TiO_2 phase during the hydrothermal annealing [14,31,32]. In the case of the carbon, it is reported that it can be interstitial or substitutional in the rutile and it can promote the formation of several localized states in the band gap and oxygen vacancies [14]. Furthermore, the dissolution of the water vapor generates hydroxyl ions, which can greatly promote the formation of oxygen vacancies in the rutile and, as a consequence, the diffusivity of oxygen ions increases [31,32].

In this work, Ti_3O_5 nano- and microfibers were obtained using the recipe reported in the mentioned previous work in order to investigate the formation of Ti(III) and Ti(IV) states on the surface and in the bulk of the Ti_3O_5 material [30].

2. Material and methods

For all of the experiments, p-type (Cz) and <100> oriented silicon samples (with resistivities from 1 to 10 Ω cm) were used. The samples were cleaned using the standard RCA procedure [30,33]. After the cleaning process, TiO_2 and C were co-deposited on bare silicon by electron beam evaporation (e-beam), and the carbon content was fixed at 3.0 wt.%.

The samples were then treated with boiling isopropanol (electronic grade from J. T. Baker) for 15 min and rinsed with de-ionized water (DI) for 5 min, since isopropanol was shown to be effective in reducing particulate levels on the surface without increasing the metal contamination content [34,35].

The base deposition pressure was maintained between 3.1×10^{-4} and 6.1×10^{-4} Pa, and the e-beam co-deposition current was 150 mA over a fixed time of 1 min, with the aim of obtaining thicknesses close to 200 nm. Thermal annealing was performed at 1000 °C in an atmosphere of nitrogen (99.2 wt.%) and water (0.8 wt.%) over 120 min. A simplified scheme of the experimental procedure is presented in process Scheme 1.

The meshes of Ti_3O_5 nano- and microfibers were characterized by a variety of techniques, including X-ray diffraction (XRD), atomic force microscopy (AFM), Fourier transform infra-red spectroscopy (FTIR), X-ray photoelectron spectroscopy (XPS), photoluminescence spectroscopy (PL) and Raman spectroscopy.

XRD analysis was performed using a model X'Pert PRO with an X'Celerator detector and a K_α line of Cu source incident at a glance angle of 0.4° and an angle range of 10–110°, with step of 0.03°. AFM images were obtained with the aid of a nanoscope with controller IIIa from Veeco in the tapping mode and the images were analyzed using the WS×M version 5.0 Develop 4.2 code [36]. FTIR spectra were obtained by a Digilab-BIO-RAD TS-4000 using an inert environment and minimizing the H_2O and CO_2 bonds due to air interference with 32 scans. The background was obtained by measuring an as-received silicon wafer (with the same doping level and resistivity that the ones used as substrate for the films).

A spectrometer for XPS (UNI-SPECS UHV) with a Mg Kα radiation ($h\nu = 1253.6$ eV) and an energy analyzer step of 10 eV under a pressure inferior than 10^{-7} Pa was used. The surface composition was determined by the relative peak areas corrected by the Scofield sensitivity

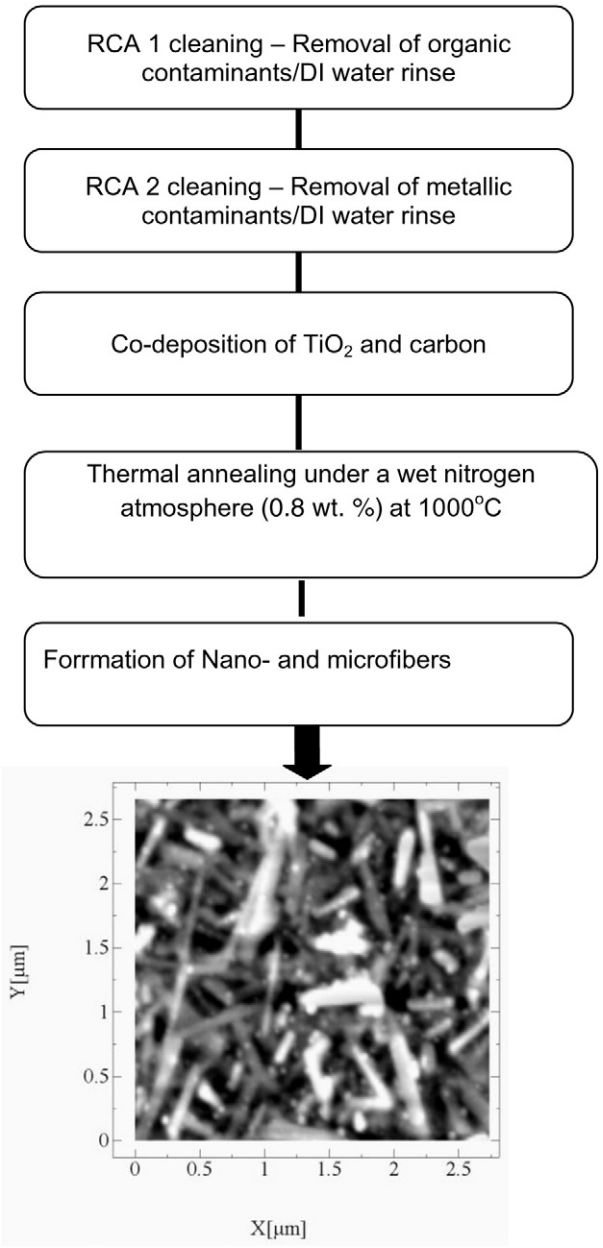

Scheme 1. Process scheme: simplified scheme of nanofiber processing.

[37] for each element. A standard sample composed by TiO_2 layer on silicon wafer was used to calibrate the equipment correcting any shift in the peak position with a precision of ±0.1 eV and the background was subtracted by Shirley method [38]. The charge correction was performed based on the binding energy of silicon dioxide Si 2p of fixed value of 103.5 eV. The width at half maximum (FWHM) varied between 1.2 and 2.1 eV. At first, a survey spectrum was obtained with a step of 0.25 eV. In case of a detailed spectrum the dwell time was set to 1 s and the step was diminished to 0.05 eV.

The PL and Raman spectra were acquired at eight different points in the same sample. PL spectra were acquired on a Renishaw System 3000, with a CCD detector and an Olympus Microscope over a wavelength range of 500 nm to 900 nm with excitation by an Ar^+ laser centered at 488 nm. Raman confocal measurements were performed on different positions along one of the samples starting from the reference level by stepping to the interface (positive shift) and to the surface (negative shift) using a 785 nm laser with 1% power, a grating of 1200 lines/mm, a 100× magnification lens and a 1 μm step.